RESEARCH

Effect of temperature on physical properties of $Bi_2Fe_4O_9$ polycrystalline materials

R. R. Awasthi[1] · B. Das[1]

Abstract

In the present study, $Bi_2Fe_4O_9$ polycrystalline powders have been prepared using standard solid-state reaction method. The function of the processing parameters such as chemical reaction, heating and cooling temperature rate, and sintering time on the single-phase formation mechanism was investigated. The prepared $Bi_2Fe_4O_9$ bulk has been sintered on different temperature from 500 to 800 °C in air to eliminate the organic impurity. The powder X-ray diffraction (PXRD) analysis confirms that $Bi_2Fe_4O_9$ bulk has typical orthorhombic phase with few intermediate impurities Fe_2O_3/Bi_2O_3. The average crystallite size of $Bi_2Fe_4O_9$ polycrystalline materials has been calculated from Scherer formula and found to be in the range of 60–100 nm. The atomic force microscopy (AFM) reveals that the spherical particles are closely packed to each other. The particle size increases with increasing the sintering temperature of $Bi_2Fe_4O_9$ bulk. The M-H measurement shows that $Bi_2Fe_4O_9$ materials have weak ferromagnetic behavior at room temperature. The dielectric constant ε' increases and the tangent loss decreases with increasing sintering temperature, which indicates that it improves the ferroelectric properties.

Keywords Bi2Fe4O9 · Magnetic · Dielectric

Introduction

During the last few decades, multiferroic materials have been attracting considerable attention, due to their coupling ferroelectric and antiferromagnetic orders in the same phase [1, 2]. Consequently, discovery of the magnetoelectric (ME) effect has been considered promising for potential applications towards developing new kinds of functional devices. There are very few energy-efficient single-phase multiferroic materials existing at room temperature [3]. The preparation of single-phase nano-structured powders is essential to enhance the ferroelectric and magnetic properties. Currently, various advanced techniques, such as the solid state reaction method [4, 5], sol-gel method [6, 7], and hydrothermal method [8, 9] have been reported to prepare multiferroic materials, which tailored the surface area to volume ratio and improved the microstructural and magnetic properties. Consequently, there is a strong interest in exploiting multiferroic materials. There are various types of multiferroic materials such as

$Bi_2M_4O_9$ (M = $Al3^+$, Ga^{3+}, In^{3+}, and Fe^{3+}) with multi-structure having attracted significant attention due to its wide scale of applications in data storage device [10–12]. Most of the multiferroic materials were observed at very low temperature with good degree of tenability. Among these multiferroics, dibismuth tetrairon oxide $Bi_2Fe_4O_9$ have attracted great interest due to its complex pentagonal symmetric structure and very strong magnetoelectric coupling, realizing extensive applications in solid-state oxide fuel. In the recent years, $Bi_2Fe_4O_9$ materials have been widely used for photocatalyst and their potential utilization of solar energy [13–15]. The $Bi_2Fe_4O_9$ material shows non-collinear magnetic arrangement with respect to magnetic frustration due to Fe^{3+} pentagonal lattice. The Fe ions in the unit cell of $Bi_2Fe_4O_9$ are evenly distributed between the tetrahedral and octahedral positions with the Bi ions coordinated by eight oxygen atoms. Some research group reported that a unit cell of $Bi_2Fe_4O_9$ consists of two kinds of Fe atoms (Fe1, Fe2) in which Fe1 occupies a tetrahedral position enclosed by four O^{2-} ions and Fe2 occupies octahedral position coordinated by six O^{2-} ions [16, 17]. The main difficulty is weak ferromagnetism and poor ferroelectric property of well-known multiferroic material, $Bi_2Fe_4O_9$, at room temperature. The partial doping at A-site or B-site or (A/B) both sites in $Bi_2Fe_4O_9$ materials has already been intensively studied and this

✉ B. Das
  bdas226010@gmail.com

[1] Department of Physics, University of Lucknow, Lucknow 226007, India

substitution shows significant improvement of its multiferroic properties [18–20]. The $Bi_2Fe_4O_9$ polycrystalline powders have been synthesized at lower temperature which increases the cation distribution enhancing the magnetic and electric polarizations simultaneously [21, 22]. The structure analysis shows that the single-phase pure and Al^{3+} doped $Bi_2Fe_4O_9$ solid solutions possess orthorhombic structure with Pbnm space group structure [23, 24]. In recent researches, it has been reported that the $Bi_2Fe_4O_9$ compounds with a tunable morphology have attracted significant interest due to its wide range of applications in actuator, solid-state oxide fuel cells, sensors and photocatalytic oxidation, etc. [11, 15, 25]. In addition, B-site doping with d-block element improving the structural, magnetic, and electric properties in multiferroic has been reported in polycrystalline $Bi_2Fe_4O_9$ [26–28]. The nanostructure $Bi_2Fe_4O_9$ materials synthesized in pure phase with different morphologies show influence in the photocatalytic properties [7, 29–31]. To the best of our knowledge, there has been no report regarding sintering temperature in order to address the above mentioned problems. The main aim of the present work is to investigate the physical properties such as structural and micro-structural changes due to increase in the sintering temperature as well as magnetic behavior of polycrystalline $Bi_2Fe_4O_9$ materials at room temperature.

Experimental details

The solid-state reaction is a most widely used method for synthesizing polycrystalline powder. The solid material necessary to heat higher temperature reacts together for the reactions. The factors such as structural properties of reactants, reactivity condition, particle size of the solids, and their reactivity and thermal free energy change related with the reaction play major roles in a solid-state reaction method. The solid-state reaction allows the reactants to chemically react, and after the reaction, it removes the residual solvent. However, it is the most convenient method because of its simplicity, low cost, and easy to add doping materials at room temperature. The polycrystalline bulk materials of $Bi_2Fe_4O_9$ were prepared by using high purity oxides Bi_2O_3 and Fe_2O_3 by standard solid-state reaction method. Both chemicals were weighted in proper amount and thoroughly mixed in stoichiometric 1:2 ratio. The Bi_2O_3 and Fe_2O_3 powders have been mixed in an agate mortar and pestle by being grounded for 3 h and calcined at 600 °C for 4 h. The chemical thermal reaction of both Bi_2O_3 and Fe_2O_3 powders can be expressed by the following:

$$Bi_2O_3 + 2\,Fe_2O_3 \rightarrow Bi_2Fe_4O_9$$

The above process was repeated 2 times for better homogeneity and phase purity of powder. Thus, uniform and homogeneous powder was converted into form of pellets using hydraulic press machine. For this, we filled a powder into die and pressed at 300 kg/cm^2 into compacted disc-shaped pellets with thickness of 2 mm and diameter 15 mm. Furthermore, the prepared pellet was put into alumina crucibles and sintered at different temperatures of 500, 600, 700, and 800 °C for 10 h respectively. The structure and phase purity of synthesized materials were confirmed by powder X-ray diffraction technique (Bruker D8 Advance) with $CuK\alpha$ radiation, $\lambda = 1.5408$ Å. The diffraction data were collected over the diffraction angle 2θ in the range of 20–70° with a scanning rate 1.5°/min. The surface morphology of as synthesized materials has been investigated by a scanning electron microscope (JEOL-JAM). The surface topography and root mean square (RMS) roughness analysis were examined by using an atomic force microscope (Digital Instrument Nanoscope–III a). Magnetic measurement hysteresis loops (M-H) were carried out using a vibrating-sample magnetometer at 300 K.

Results and discussion

X-ray diffraction analysis

Figure 1 shows the XRD patterns of dibismuth tetrairon nonaoxide $Bi_2Fe_4O_9$ materials synthesized by the solid-state reaction method. The XRD patterns are perfectly well matched and all assign diffraction peaks were indexed with standard JCPDS no. 80-8638. It is well indexed and all major peaks belong to the orthorhombic crystal structure with Pbam space group. Thus, X-ray diffraction pattern of dibismuth tetrairon nonaoxide confirms the existence of orthorhombic phase sintered pellet at temperature 500 °C in air for 10 h. After being sintered at temperature 600 °C in open air for 10 h, the XRD pattern shows slightly increase in crystallinity of $Bi_2Fe_4O_9$ materials. Further increasing the sintering temperature to 700 °C, the doublet peak intensity gradually decreases and transforms into a single peak, which shows gradual structural phase transformation. On the other hand, further increasing the sintering temperature from 700 to 800 °C, the diffraction peak intensity increase shows that the crystallinity of $Bi_2Fe_4O_9$ materials increases. The lattice parameters of $Bi_2Fe_4O_9$ pellet sintered at 500 °C were calculated and found to be a = 7.984 Å, b = 8.475 Å, and c = 5.993 Å. With increasing the sintering temperature from 500 to 600 °C, the lattice parameters change to a = 7.987 Å, b = 8.465 Å, and c = 5.998 Å. Further increasing the sintering temperature from 600 to 700 °C, the lattice parameters change to a = 7.990 Å, b = 8.469 Å, and c = 6.018 Å. Furthermore, increasing the sintering
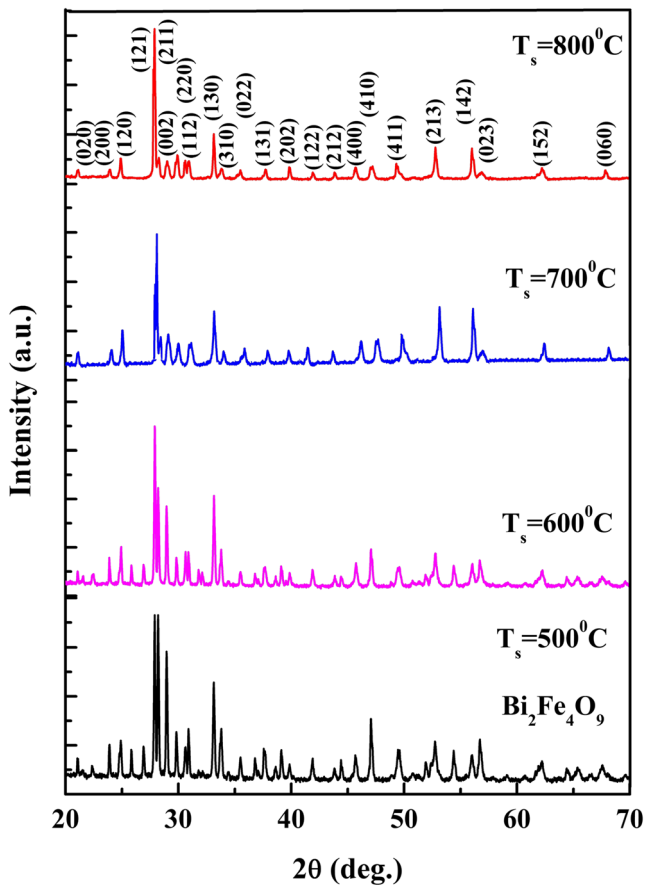
Fig. 1 Powder XRD patterns of $Bi_2Fe_4O_9$ polycrystalline materials sintered at temperatures ranging from 500 °C to 800 °C

temperature from 700 to 800 °C, the lattice parameters change to a = 7.998 Å, b = 8.465 Å, and c = 6.056 Å. The mean crystallite size D of the sample powder was deduced from the full width at half maximum using the Scherer formula.

$$D = \frac{K\lambda}{\beta\cos\theta} \qquad (1)$$

where K is constant, and for the spherical shape, its value is 0.9; λ is the wavelength of X-ray; β is the full width at half maxima (FWHM); and θ is the diffraction angle. The average crystallite size of $Bi_2Fe_4O_9$ polycrystalline material sintered from various temperatures, 500 to 800 °C, was calculated and found to be ~ 60–100 nm. The crystallite size of $Bi_2Fe_4O_9$ polycrystalline material increases with increasing sintering temperature.

The more accurate crystallite size and lattice strain of each thin film were calculated using Williamson-Hall (W-H) plots. The mathematical relation between the integral full width at half maxima (β), lattice microstrain (ε), and crystallite size (D) is given as follows:

$$\beta\cos\theta = \frac{k\lambda}{D} + 4\varepsilon\sin\theta \qquad (2)$$

The Bragg diffraction peak width is a combination of instrumental integral width and the width broadening due to the materials. Therefore, the correct broadening of the diffraction peak of BFO thin films is estimated using the relation

$$\beta = \left[\beta_{measure}^2 - \beta_{instrumental}^2\right]^{1/2} \qquad (3)$$

The instrumental integral width ($\beta_{instrumental}$) was determined from the collected diffraction data of a standard material such as silicon. Furthermore, the linear fit to the data of the graph plotted between $\beta\cos\theta$ and $4\sin\theta$ (known as Williamson-Hall plots), the inverse of intercept gives the value of crystallite size (D) and the slope gives the value of the lattice strain (ε). The values of the lattice strain have been calculated from the W-H plot and found to be 9.14×10^{-3}, 3.52×10^{-3}, 3.79×10^{-3}, and 1.86×10^{-3} of $Bi_2Fe_4O_9$ materials sintered from 500 °C, 600 °C, 700 °C, and 800 °C respectively. Therefore, increasing the sintering temperature decreases the lattice strain. The crystallite sizes are calculated from the Scherrer formula and obtained from the W-H plot; it was found to be close to each other.

Surface morphological analysis

The morphological studies of sintered $Bi_2Fe_4O_9$ multiferroic materials have been carried out by a scanning electron microscopy (SEM) technique. The SEM micrograph of $Bi_2Fe_4O_9$ materials sintered from 500 to 800 °C is shown in Fig. 2a–d. The micrograph revealed that $Bi_2Fe_4O_9$ materials mostly consist of spherical shape grain and each grain is interconnected edge by edge. Due to increase in the sintering temperature, grain size is found to increase from ~ 70 to ~ 300 nm. With increasing sintering temperature, grain size increases, which may be attributed to the oxygen vacancies. This increase of grain size and crystalline character with increasing sintering temperature is also evident from XRD studies as well. The EDAX spectrum also shows that existing Bi, Fe, and O elements and content increases with increasing the sintering temperature are shown in Fig. 3a and b.

Surface topographic analysis

Atomic force micrographs of $Bi_2Fe_4O_9$ materials are shown in Fig. 4a–d. These micrographs are showing that particle size increases with increasing sintering temperature from 500 to 800 °C. The above investigations also revealed that the particles are closely packed and pores between the particles are very few. The root mean square (RMS) roughness was calculated and found to be 13.59, 12.34, 29.88, and 21.68 nm. The particle size shown by AFM/SEM is higher as compared with

Fig. 2 FESEM images of $Bi_2Fe_4O_9$ polycrystalline materials sintered at various temperatures such as (**a**) 500 °C, (**b**) 600 °C, (**c**) 700 °C and (**d**) 800 °C
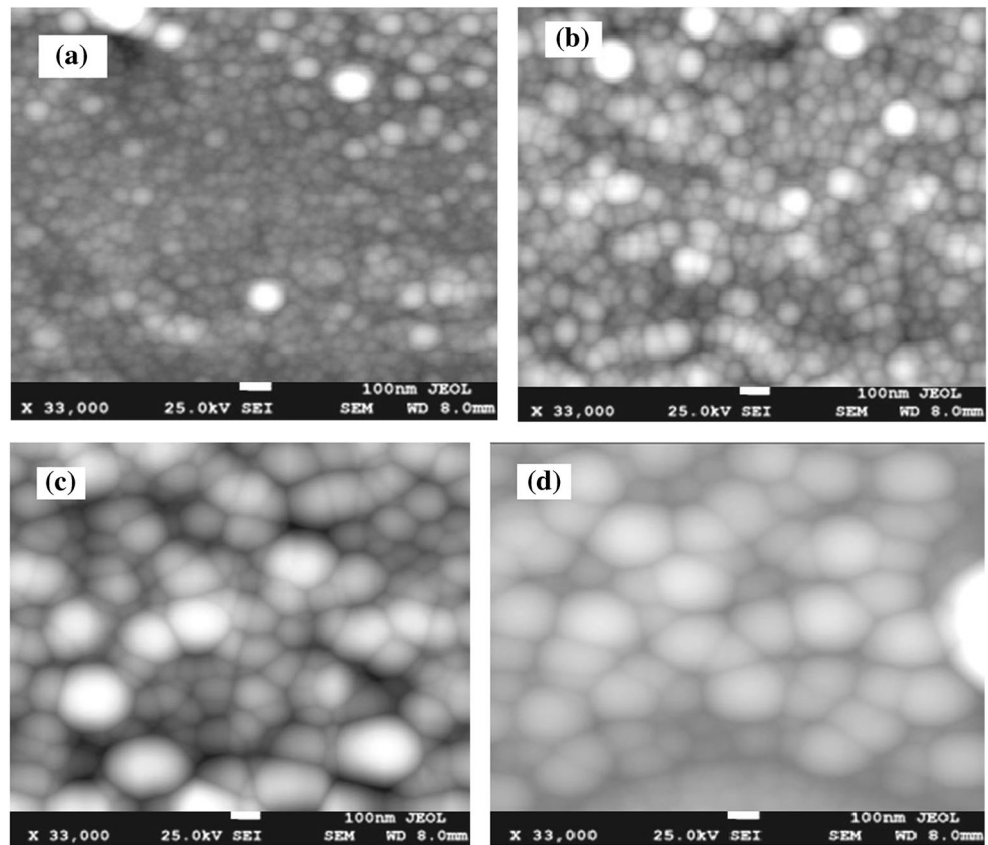

Fig. 3 EDAX spectra of $Bi_2Fe_4O_9$ materials sintered at temperature of (**a**) 500 °C and (**b**) 800 °C showing the presence of Bi, Fe, and O elements and their content increases with increasing sintering temperature
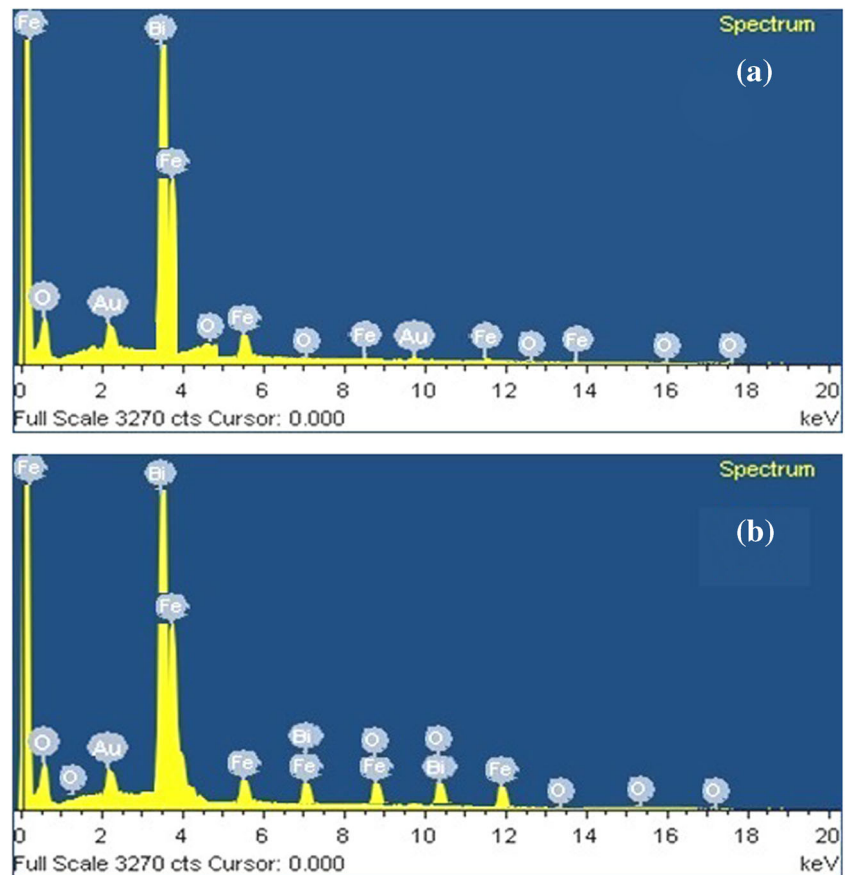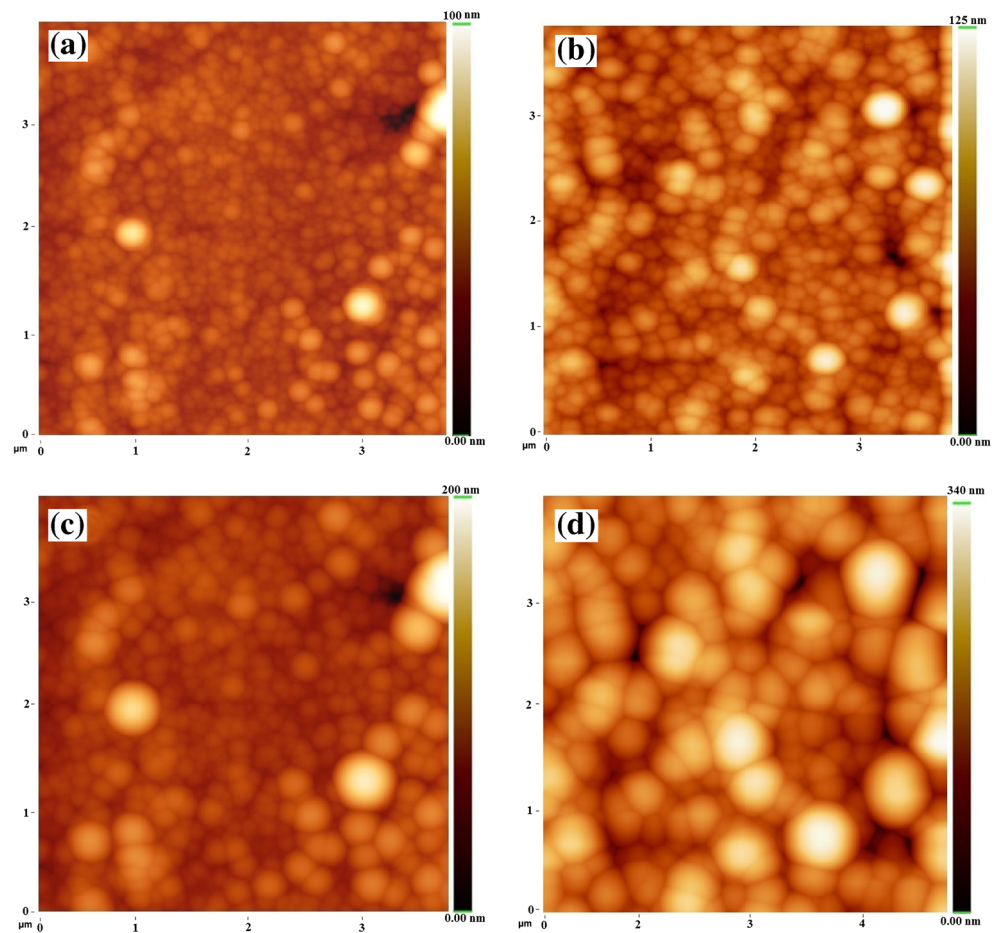
Fig. 4 AFM images of $Bi_2Fe_4O_9$ polycrystalline materials sintered at various temperatures such as (**a**) 500 °C, (**b**) 600 °C, (**c**) 700 °C, and (**d**) 800 °C

that calculated from the XRD results. This is because of the fact that the XRD gave the average mean crystallite size while AFM/SEM showed agglomeration of the crystallites.

Magnetic properties

In $Bi_2Fe_4O_9$ materials, each octahedral Fe_1 atom is surrounded by six oxygen atoms (FeO_6) and each tetrahedral Fe_2 atom is surrounded by four oxygen atoms (FeO_4). The spins of tetrahedral (FeO_4) atom are parallel to the octahedral (FeO_6) atom but the spins of the octahedral (FeO_6) atoms are parallel to the nearest octahedral (FeO_6) atom (shown in inset Fig. 5), causing spin frustration in $Bi_2Fe_4O_9$ materials. Figure 5 shows hysteresis loops of magnetization (M) vs. magnetic field (H) at room temperature of $Bi_2Fe_4O_9$ materials. The M-H hysteresis loops of $Bi_2Fe_4O_9$ materials show weak ferromagnetic behavior at room temperature. The observed value of remnant magnetization and coercivity are found to be ~ 0.015 emu/g and 67.59 emu/g at room temperature. The unsaturated M-H loops are the consequence of weak ferromagnetism due to spin frustration.

MFM analysis

The local magnetic domain structure of BFO thin films has been studied using high-resolution magnetic force microscopy (MFM). Figure 6a and b show the MFM phase image of $Bi_2Fe_4O_9$ materials sintered from 500 to 800 °C. The bright-dark dipole contrast appearing in the MFM phase image clearly shows the presence of magnetic domains. Also, the bright-dark dipole contrast into the dark contrast varies due to rotation of magnetization axis. In order to know further about the uniformity of the magnetic domain distribution, the MFM phase images and their corresponding cross-sectional analysis were also recorded. The cross-sectional phase contrast shown in Fig. 6c and d, sintered at 500 °C and 800 °C, changes from + 0.3° to − 0.4° and + 0.32° to − 0.44° respectively. Interestingly, the increased phase contrast shows improved magnetoelectric coupling.

Dielectric analysis

The frequency-dependent dielectric properties of $Bi_2Fe_4O_9$ bulk materials have been measured in the frequency range of 0.1 kHz to 1 MHz with room temperature. To study the

Fig. 5 M-H polt of $Bi_2Fe_4O_9$ polycrystalline materials sintered at 800 °C.The inset shows the spins of tetrahedral (FeO_4) atom parallel to the octahedral (FeO_6) atom
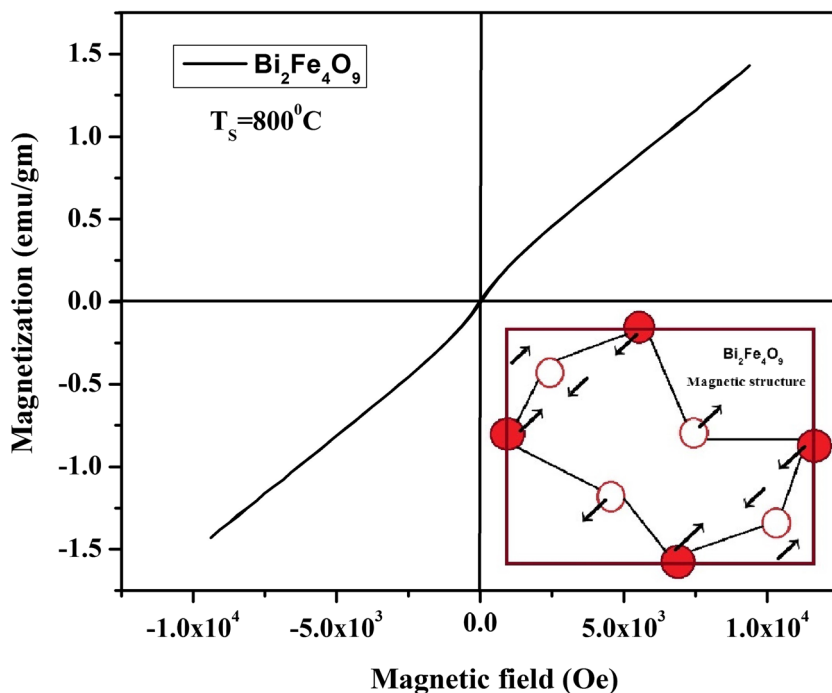
dielectric properties of $Bi_2Fe_4O_9$ polycrystalline materials sintered with various temperatures from 500 to 800 °C, measured complex impedance parameters such as capacitance Cp and conductance G are as follows.

$$C_0 = \varepsilon_0 \frac{A}{d} \tag{4}$$

$$\varepsilon' = \frac{C_p}{C_0} \tag{5}$$

Fig. 6 The MFM phase images (**a** & **b**) and their corresponding cross sectional phase images (**c** & **d**) of $Bi_2Fe_4O_9$ materials sintered at 500 °C and 800 °C
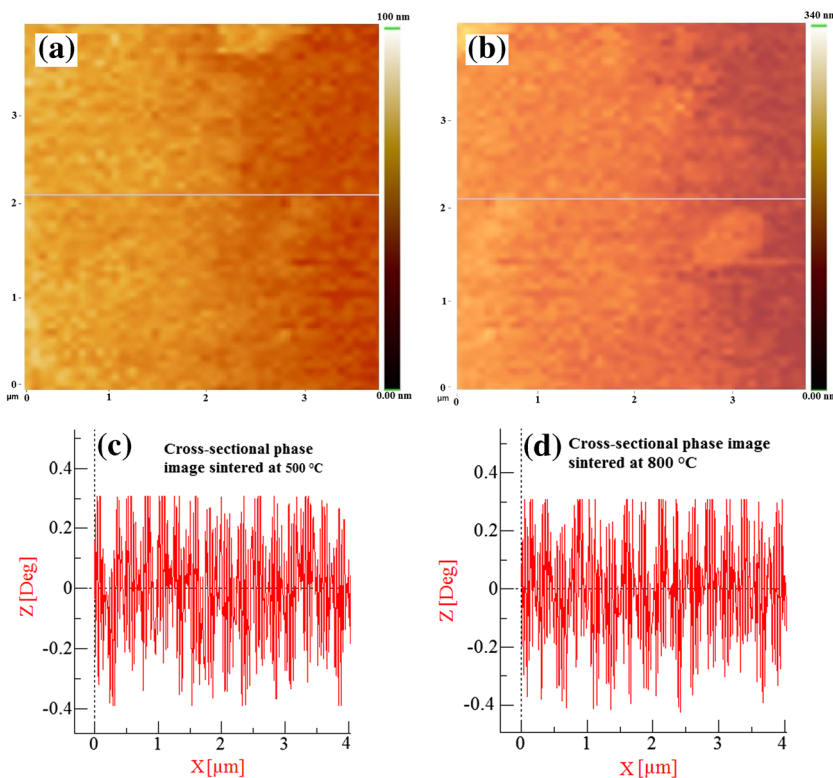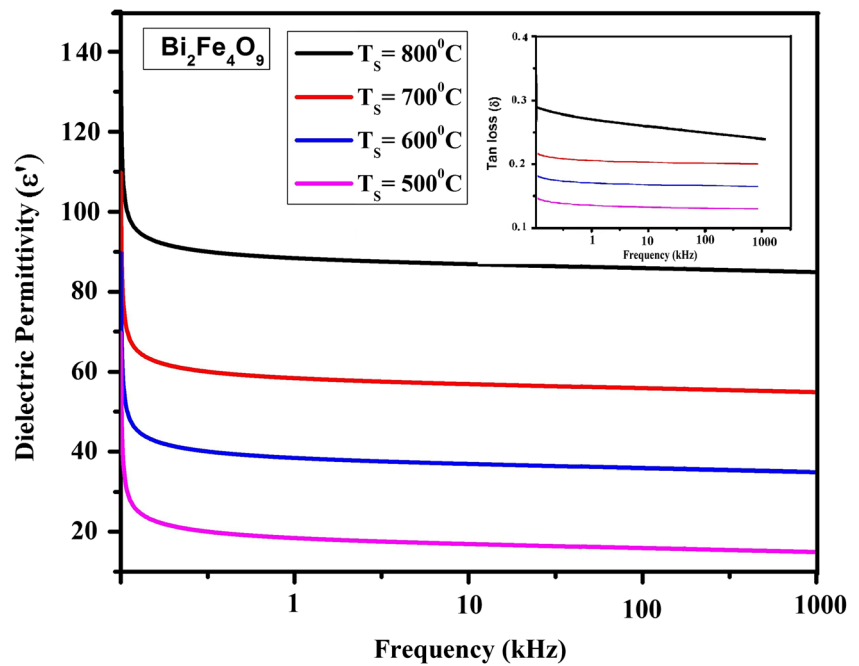
Fig. 7 The variation of dielectric permittivity (ε') and tan loss (inset) as a function of frequency for $Bi_2Fe_4O_9$ materials sintered at (**a**) 500 °C, (**b**) 600 °C, (**c**) 700 °C and (**d**) 800 °C

$$\varepsilon'' = \frac{G}{\omega C_0} \tag{6}$$

Complex dielectric constant

$$\varepsilon^* = \varepsilon' - j\varepsilon'' \tag{7}$$

Tangent loss

$$\tan\delta = \frac{\varepsilon''}{\varepsilon'} \tag{8}$$

where ε_0 is the permittivity of vacuum, A is the area of sintered pellet, d is the thickness of pellet, and $\omega = 2\pi f$ is the angular frequency. The variations of dielectric constant (ε') as a function of frequency are presented in Fig. 7. It is observed from Fig. 7 that dielectric constant (ε') decreases with increasing frequency and almost flattens at high frequency due to dielectric relaxations. The value of dielectric constant (ε') of $Bi_2Fe_4O_9$ bulk materials with sintering from 500 to 800 °C has been calculated at frequency of 1 MHz and found to be 20, 40, 60, and 90. As shown in Fig. 7, dielectric constant ε' relatively increases with increasing sintering temperature confirming that it exhibits space charge polarization. It is also observe that tangent loss decreases with increasing sintering temperature; it can be explained with the help of the Maxwell-Wagner effect. Generally, the dipolar, electronic, ionic, and interfacial polarizations contribute to the dielectric constant of any material. At low frequencies, the dipolar and interfacial polarizations are effective to the dielectric constant. However, at higher frequencies, the electronic polarization is effective and the dipolar contribution becomes insignificant. The

decrease in dielectric constant with increased frequency could be explained on the basis of dipole relaxation phenomenon. Hence, increasing the sintering temperature, which decreases the point defects such as oxygen vacancies, attributed to the decrease of the leakage current density.

Conclusion

The analysis of XRD patterns revealed that $Bi_2Fe_4O_9$ polycrystalline materials crystallize in the orthorhombic phase with the Pbnm space group. The lattice parameter and crystallite size (60–100 nm) increase with increasing sintering temperature from 500 to 800 °C. Surface morphological investigation examined with the help of SEM/AFM micrograph revealed that the spherical grains are well connected to each other with clear grain and grain boundary. With increasing the sintering temperature, grain growth increases and the pores between the grains decreases. The M-H measurement revealed that $Bi_2Fe_4O_9$ bulk shows weak ferromagnetic behavior at room temperature. The dielectric constant ε' relatively increases and tangent loss decreases with increasing sintering temperature which indicates improvement in the ferroelectric properties of multiferroic materials. Future research will focus on the investigation of physical property (ME) and (P-E) measurements of multiferroic properties.

References

1. Lawes, G., Srinivasan, G.: J. Phys. D. Appl. Phys. **44**, 243001–243022 (2011)
2. Ma, J., J, H., Li, Z., Nan, C.W.: Adv. Mater. **23**, 1062–1087 (2011)
3. Zhou, C.C., Luo, B.C., Jin, K.X., Cao, X.S., Chen, C.L.: Solid State Commun. **150**, 1334–1337 (2010)
4. Singh, A.K., Kaushik, S.D., Kumar, B., Mishra, P.K., Venimadhav, A., Siruguri, V., Patnaik, S.: Appl. Phys. Lett. **92**, 132910–132913 (2008)
5. Koizumi, H., Niizeki, N., Ikeda, T.: Jpn. J. Appl. Phys. **3**, 495–496 (1964)
6. Liu, T., Xu, Y., Zeng, C.: Mater. Sci. Eng. B. **176**, 535–539 (2011)
7. Yang, Z., Huang, Y., Dong, B., Li, H.L., Shi, S.Q.: J. Solid State Chem. **179**, 3324–3329 (2006)
8. Xiong, Y., Wu, M.Z., Peng, Z.M., Jiang, N., Chen, Q.W.: Chem. Lett. **33**, 502–503 (2004)
9. Wang, Y.G., Xu, G., Yang, L.L., Ren, Z.H., Wei, X., Weng, W.J., Du, P.Y., Shen, G., Han, G.R.: Ceram. Int. **35**, 51–53 (2009)
10. Ruan, Q.-J., Zhang, W.-D.: J. Phys. Chem. C. **113**, 4168–4173 (2009)
11. Zhang, M., Yang, H., Xian, T., Wei, Z.Q., Jiang, J.L., Feng, Y.C., Liu, X.Q.: J. Alloys Compd. **509**, 809–812 (2011)
12. Scott, J.F.: Nat. Mater. **6**, 256–257 (2007)
13. Liu, Z.S., Wu, B.T., Zhu, Y.B.: Mater. Chem. Phys. **135**, 474–478 (2012)
14. Han, J.T., Huang, Y.H., X J, W., Wu, C.L., Wei, W., Peng, B., Huang, W., Goodenough, J.B.: Adv. Mater. **18**, 2145–2148 (2006)
15. Schneider, H., Fischer, R.X., Gesing, T.M., Schreuer, J., Mühlberg, M.: Int. J. Mater. Res. **103**, 422–429 (2012)
16. Ressouche, E., Simonet, V., Canals, B., Gospodinov, M., Skumryev, V.: Phys. Rev. Lett. **103**, 267204 (2009)
17. Mohapatra, S.R., Sahu, B., Badapanda, T., Pattanaik, M.S., Kaushik, S.D., Singh, A.K.: J. Mater. Sci. Mater. Electron. **27**, 3645–3652 (2015)
18. Miao, J.H., Fang, T.-T., Chung, H.-Y., Yangz, C.-W.: J. Am. Ceram. Soc. **92**, 2762–2764 (2009)
19. Raghavan, C.M., Kim, J.W., Choi, J.Y., Kim, J.-W., Kim, S.S.: Ceram. Int. **40**, 14165–14170 (2014)
20. Ray, J., Biswal, A.K., Acharya, S., Ganesan, V., Pradhan, D.K., Vishwakarma, P.N.: J. Magn. Magn. Mater. **324**, 4084–4089 (2012)
21. Zhaoa, J., Liua, T., Xua, Y., Hea, Y., Chenb, W.: Mater. Chem. Phys. **128**, 388–391 (2011)
22. Huang, S., Qiu, Y., Yuan, S.L.: Mater. Lett. **160**, 323–326 (2015)
23. Huang, S., Shi, L.R., Tian, Z.M., Yuan, S.L., Zhu, C.M., Gong, G.S., Qiu, Y.: J. Solid State Chem. **227**, 79–86 (2015)
24. Da Silva, K.L., Sepelak, V., Paesano Jr., A., Litterst, F.J., Becker, K.-D.: Z. Anorg. Allg. Chem. **636**, 1018–1025 (2010)
25. Sun, S.M., Wang, W.Z., Zhang, L., Shang, M.: J. Phys. Chem. C. **113**, 12826–12831 (2009)
26. Liu, M., Yang, H., Yang, Y.L.Y.: J. Mater. Sci. Mater. Electron. **25**, 4949–4953 (2014)
27. Dutta, D.P., Sudakar, C., Mocherla, P.S.V., Mandal, B.P., Jayakumar, O.D., Tyagi, A.K.: Mater. Chem. Phys. **135**, 998–1004 (2012)
28. Mao, X., Sun, H., Wang, W., Y, L., Chen, X.: Solid State Commun. **152**, 483–487 (2012)
29. Wang, X., Zhang, M., Tian, P., Chin, W.S., Zhang, C.M.: Appl. Surf. Sci. **321**, 144–149 (2014)
30. Park, T.J., Papaefthymion, G.C., Moodenbuugh, A.R., Mao, Y., Wong, S.S.: J. Mater. Chem. **15**, 2099–2105 (2005)
31. Zhang, X.Y., Lv, J., Bourgeois, L., Cui, J., Wu, Y.C., Wang, H.T., Webley, P.A.: New J. Chem. **35**, 937–941 (2011)